

Fermi National Accelerator Laboratory

FERMILAB-PUB-91/76-T

MAD/PH/638

FSU-HEP-910404

April 1991

A Comparative Study of the Benefits of Forward Jet Tagging in Heavy Higgs Production at the SSC

V. Barger,¹ Kingman Cheung,¹ T. Han,² J. Ohnemus,³ D. Zeppenfeld¹

¹*Department of Physics, University of Wisconsin, Madison, WI 53706*

²*Fermi National Accelerator Laboratory, P. O. Box 500, Batavia, IL 60510*

³*Department of Physics, Florida State University, Tallahassee, FL 32306*

ABSTRACT

The event rate for production of a Higgs boson of mass ~ 1 TeV with decay $H \rightarrow ZZ \rightarrow 4$ charged leptons is of order 25 events per year at standard SSC luminosity and the QCD background is of comparable size. By tagging a *single* forward jet of energy $E_j > 1$ TeV and rapidity $2 < |\eta_j| < 5$ from the $qq \rightarrow qqZZ$ process, the QCD background can be essentially eliminated, with about 10 Higgs signal events per year remaining, which amounts to 70% of the $qq \rightarrow qqZZ$ signal rate. The complete experimental separation of the vector boson scattering subprocess is thereby possible.



I. INTRODUCTION

A primary goal of the SSC and the LHC is to search for the Higgs boson which is the relic of electroweak symmetry breaking in the Standard Model (SM). Since the Higgs mass is unknown, one must be prepared to search over a mass range at least up to $m_H = 1$ TeV and possibly beyond for strong WW scattering effects if a resonant scalar state is not found. For a Higgs boson of mass $m_H > 2M_Z$, the decay mode of principal interest has been $H \rightarrow ZZ$, since the $Z \rightarrow e\bar{e}$, $\mu\bar{\mu}$, and $\nu\bar{\nu}$ decay modes provide distinctive signatures. The production processes for a heavy Higgs boson ($m_H > 2M_Z$) are $gg \rightarrow ZZ$ and $qq \rightarrow qqZZ$ with the Higgs boson appearing as an intermediate state in some of the Feynman diagrams.

For a top mass of order 140 GeV the cross-section for the gg initiated process dominates that of qq up to $m_H \sim 1$ TeV. Thus, at first sight, it would seem that jet-inclusive ZZ events offer the best approach to Higgs boson discovery. However, the width of a Higgs boson with $m_H \sim 1$ TeV is so broad that the s -channel resonant structure is lost. Moreover the QCD backgrounds to the jet-inclusive final state are of comparable size. The theoretical uncertainty inherent in the QCD background limits the significance by which the signal can be established.

In contrast, the forward jets in the $qq \rightarrow qqZZ$ process provide a means to enhance the signal over background by judicious jet selection criteria. Jet tagging techniques have been previously discussed with the aim of isolating the Higgs signal.¹ For the $qq \rightarrow qqZZ \rightarrow qql\bar{l}\bar{l}$ case, with a distinct four-charged lepton signature, there is in principle no need to tag the spectator jets² when $m_H < 0.6$ TeV. However, for a Higgs boson of mass $m_H \sim 1$ TeV, the event rate at the SSC from $gg \rightarrow ZZ$ is low, and the presence of the irreducible QCD background may preclude a statistically significant observation in the inclusive channel. Thus if a clean signal is possible through jet tagging of the $qq \rightarrow qqZZ$ process, this channel becomes interesting in its own right to study a heavy Higgs boson or alternatively strong vector boson scattering.³

In this paper we compare the prospects for finding a heavy Higgs boson signal in jet-

inclusive and jet-tagged ZZ processes. We find that jet-tagging yields an advantageous signal/background ratio for finding a Higgs boson of mass $m_H \sim 1$ TeV at the SSC and that the significance of a heavy Higgs signal can be improved considerably.

II. CALCULATIONAL METHODS

The SM ZZ signals and backgrounds for the Higgs boson have been extensively studied in the literature. For the purpose of this study a variety of processes need to be considered.

A. Continuum ZZ Production

To lowest order, ZZ production occurs via the subprocess $q\bar{q} \rightarrow ZZ$ which is shown in Fig. 1(a) and which was first calculated by Brown *et al.*⁴ The full $\mathcal{O}(\alpha_s)$ QCD corrections for this continuum ZZ production process have been calculated recently.^{5,6} For the jet-inclusive ZZ production rate we use the calculation of Ohnemus and Owens⁶ which allows us to impose acceptance cuts on the Z -bosons. Compared to the previously available tree level results, uncertainties arising from the arbitrariness in the scale choice for the strong coupling constant α_s and for the parton structure functions are substantially reduced. We choose a scale $Q^2 = M_{ZZ}^2$ in both the strong coupling constant α_s and in the structure functions for all our QCD background calculations. Here M_{ZZ} is the invariant mass of the produced Z boson pair. For the parton distribution functions we use the parameterization HMRS(B) of Harriman *et al.*⁷ throughout this paper.

Contained in the jet-inclusive calculation are the tree-level $ZZ + 1$ parton production processes^{8,9} which are indicated in Fig. 1(b). These tree-level results for $ZZ + 1$ jet production are the basis for our estimates of the QCD background to single jet tagging. Gluon emission as depicted in Fig. 1(b) leads to both infrared and collinear singularities in the tree level cross section formulas. These singularities can be avoided by implementing experimental acceptances in the calculation. We impose a cut of $E_j > 100$ GeV on the jet energy as measured in the lab frame in order to regularize the soft divergencies. The collinear singularities are eliminated by requiring the jet to appear at a pseudorapidity $|\eta_j| < 5$.

In discussing infrared singularities the parton center of mass system is the relevant reference frame. If the laboratory frame involves a large boost along the beam axis from the center of mass frame then a soft gluon emission can give rise to a large jet energy, but at low transverse momentum (p_T); hence this infrared singular behaviour is eliminated by a p_T cut. However, if acceptance cuts restrict the Z -bosons to the central region, then the $ZZ + 1$ jet kinematics preclude the possibility that a soft jet gets a high boost. Consequently a minimum energy cut on the jet is then sufficient as a regulator. The main motivation for our method of regularizing the singular regions is enhancement of the signal to background ratio. It differs from the conventional approach of using a jet p_T cut as a regulator.^{8,9}

Our starting choice of acceptance cuts on the jet energy and pseudorapidity,

$$E_j > 100 \text{ GeV} , \quad |\eta_j| < 5, \quad (1)$$

along with cuts on the Z transverse momenta, rapidities, and ZZ invariant mass that define the heavy Higgs search region,

$$p_{TZ} > \frac{1}{4} \sqrt{M_{ZZ}^2 - 4M_Z^2} , \quad |y_Z| < 2.5 , \quad M_{ZZ} > 500 \text{ GeV} , \quad (2)$$

leads to a $ZZ + 1$ jet cross section which almost saturates the jet inclusive ZZ rate to $\mathcal{O}(\alpha_s)$. Hence our jet energy distributions for the continuum QCD background should only be taken as a rough estimate of the true rate in the vicinity of the cutoff value for E_j . This caveat does not apply in the high E_j tagging region where we will be safely away from the soft emission singularities. We estimate an uncertainty of a factor 2 or less in these background evaluations (associated with the scale ambiguity inherent in tree-level calculations and the as yet unknown K -factor of the $ZZ + 1$ jet cross section).

When double jet tagging is contemplated one has to consider QCD backgrounds arising from additional hard gluon radiation in the processes of Fig. 1(b) as well as the novel contributions as indicated in Fig. 1(c). All QCD processes leading to $ZZ + 2$ jet production have been calculated at the tree level by Barger *et al.*⁹ and confirmed by Baur and Glover.¹⁰ In some of these dijet production processes an additional singularity appears when the two

final state massless partons are collinear. This singularity is regularized at the tree level by imposing a separation requirement $R_{jj} > 0.7$ in the azimuthal angle pseudorapidity plane; SSC detectors will be easily capable of such a jet-jet separation.

B. $gg \rightarrow ZZ$

Even though formally suppressed by two powers of the strong coupling constant α_s , the gluon-gluon fusion contribution to ZZ production is sizable because of the high density of gluons inside the proton. The Feynman graphs for this process are depicted in Fig. 2 and include the triangle graph which leads to Higgs production via a top-quark loop. These gluon fusion processes have been calculated by Dicus *et al.*¹¹ and by Glover and van der Bij.¹² We use the calculation of Ref. 12 in the following. The size of the Higgs production cross section critically depends on the top quark mass m_t ; we take $m_t = 140$ GeV as a representative value throughout this work. The scale in α_s and in the structure functions is chosen to be $Q^2 = M_{ZZ}^2$ for the gluon fusion process.

C. $qq \rightarrow qqZZ$ via Electroweak Processes

At $\mathcal{O}(\alpha^4)$, electroweak processes contribute significantly to ZZ production in association with two (anti)quarks giving rise to up to two visible jets. An incomplete set of Feynman graphs for these processes is shown in Fig. 3. The major interest here is in the scattering of longitudinal vector bosons occurring in subprocesses such as the ones shown in Fig. 3(a). This includes the Higgs boson resonance. Our goal is to isolate this ‘signal’ from the continuum ZZ production discussed earlier by detecting the presence of a high energy but relatively low p_T spectator quark jet in the virtual electroweak boson emission process.

For a full tree-level calculation of $ZZqq$ production the contributions to ZZ production in which the Z -bosons are radiated from external quark lines must also be considered (see Figs. 3(b) and 3(c)). A large set of gauge invariant diagrams of these electroweak processes has been evaluated previously by Dicus *et al.*¹³ and a full calculation was presented by Baur and Glover.¹⁰ We have independently performed a full calculation of these processes using

the helicity amplitude techniques of Ref. 14 and find numerical agreement with the previous results. A full discussion of all contributing Feynman graphs and compact expressions of our amplitudes are given in Appendix A.

All our results are obtained with a Breit-Wigner form of the Higgs-propagator for s -channel Higgs boson exchange as in Fig.3(a), with an s -independent width Γ_H . The effect of s -dependence of the width is to shift the effective Higgs boson mass downward and to modify the shape of the resonance contribution¹⁵. With such an s -dependence of the width, the event rate would be larger than for our constant width calculation.

In the dominant electroweak contribution which arises from the vector boson fusion graphs of Fig.3(a) the process as seen by each of the two incoming protons is like that of deep inelastic lepton-proton scattering. This strongly suggests a scale choice related to the average virtuality of the incoming weak bosons in the structure functions. In this spirit we use $Q^2 = M_W^2$ as the scale in the calculation of the electroweak signal processes.

Since we are also interested in the size of the electroweak signal processes when no or only one of the final state quarks appears as a jet, singular phase space regions which are associated with the exchange of massless photons in the $qq \rightarrow qqZZ$ process have to be carefully scrutinized. Two cases need to be considered. The first is the t -channel photon exchange represented by the Feynman graph of Fig. 3(b). At very low Q^2 of the photon the process is effectively $\gamma + q \rightarrow Z + Z + q$ and the deep inelastic scattering approximation breaks down. Consequently we require $Q^2 > 5 \text{ GeV}^2$ for the t -channel photon propagator in our calculation. The phase space region below $Q^2 = 5 \text{ GeV}^2$ may contribute to high p_T Z pair production, similar to new particle production processes in ep scattering involving elastic emission of photons off the proton.¹⁶ In order to estimate the contribution to $ZZ + \text{jet}(s)$ production from the low Q^2 region we have calculated the cross section for the elastic process $pp \rightarrow p + ZZ + \text{jet} + X$ using the techniques described in Ref. 16. Details of the calculation are given in Appendix B. We find a cross section of $\sigma = 0.12 \text{ fb}$ for this semi-elastic contribution, which is 3 orders of magnitude smaller than the full $\mathcal{O}(\alpha^4)$ electroweak contribution with

$m_H = 0.1 \text{ TeV}$; the resonant production cross section $pp \rightarrow N^* + ZZ + \text{jet} + X$ will be similarly negligible.

Finally we note that the collinear singularity in creation of $\bar{q}q$ pairs from low Q^2 photons, as depicted in Fig. 3(c) is eliminated by imposing an $R_{jj} > 0.7$ separation cut on the final state partons, as was used for the 2-jet QCD background calculation.

We are primarily interested in the electroweak contribution due to a heavy Higgs boson or other longitudinal weak boson scattering mechanisms. In this context the production of transversely polarized Z bosons may be considered as an ‘electroweak background’. Because of important interference effects between all contributing Feynman graphs, the Higgs contribution cannot be directly isolated. Rather, we use the SM prediction with a light Higgs boson ($m_H = 0.1 \text{ TeV}$), where the Z bosons are primarily transverse, as a definition of the electroweak background to the Higgs signal.

III. SINGLE JET TAGGING

In jet-inclusive ZZ production there is little that one can do to separate the Higgs signal from the continuum background except to require central Z ’s and to make a p_T cut, $p_{TZ} > \frac{1}{4}\sqrt{M_{ZZ}^2 - 4M_Z^2}$, that enhances the Jacobian peak region of $H \rightarrow ZZ$ decay. In contrast, the jet activity in the $qq \rightarrow qqZZ$ process provides a powerful means to separate the Higgs signal from the QCD background. At least one of the final state quark jets is very energetic and largely at forward angles, unlike the jets from the QCD continuum which have lower energy because of the infrared singularities occurring in gluon emission.

To analyze the practicality of jet tagging, we first consider the rather minimal requirements of Eq. (1) on the jet energy and jet rapidity in the lab frame, as discussed in Sec. 2. For the $qq \rightarrow qqZZ$ process only one jet is required to satisfy Eq. (1). In the case that two jets satisfy Eq. (1), the most energetic jet is used in the following. Figure 4 gives the distribution $d^2\sigma/dE_j d\eta_j$ for the signal and the QCD background. We observe that the signal events occur dominantly above $E_j \approx 1 \text{ TeV}$ and the background is mostly below this jet energy.

In addition, the signal is concentrated at large rapidities, $|\eta_j| \gtrsim 2$, while the background is more or less uniformly distributed in rapidity. These features are evident in Fig. 5 where the jet rapidity distributions $d\sigma/d\eta_j$ are compared for the jet energy requirements of $E_j > 100, 500$ and 1000 GeV. We enhance the signal/background ratio, with little cost to the signal event rate, by the criteria

$$E_j > 1000 \text{ GeV} , \quad 2 < |\eta_j| < 5 . \quad (3)$$

The above discussion pertains to single jet tagging only. One may ask whether further improvements can be achieved by also considering the second jet of the signal. To this end, we compare the energy distribution of the secondary jet having rapidity satisfying Eq. (1), but in the opposite hemisphere. Figure 6 compares the $d\sigma/dE_j$ distributions of the tagged and secondary jets for both the signal and the background. Note that the E_j distribution of the secondary jet is much softer than that of the primary jet; hence any E_j cut on the secondary jet higher than 100 GeV will considerably reduce the signal event rate. Moreover the requirement of a second jet in the $2 < |\eta_j| < 5$ rapidity range already reduces the signal rate by 25%. We conclude that double jet tagging is not useful because of the reduction of the already small signal.¹⁷

Returning to the single jet tagging, the E_j distributions are summarized in Fig. 7, with $d\sigma/dE_j$ shown in (a) and $\sigma(E_j > E_{\text{cut}})$ given in (b). By imposing the $E_j > 1$ TeV cut, the QCD background is reduced by a factor of 10 below the $m_H = 1.0$ TeV signal. Thus we are left with the desirable situation of a nearly background-free electroweak signal. The QCD background falls steeply with increasing E_j whereas the signals have a very hard E_j spectrum; see Fig. 7(a). Hence a heavy Higgs boson will be revealed by a sharp break in the jet energy distribution near $E_j \sim 500\text{--}750$ GeV. The fact that the signal appears as a distinct break in the E_j distribution means that its discovery is not dependent on a precise calculation of the QCD background as is the case in the jet-inclusive search.

It is of interest to also examine the p_T distribution of the tagged jet. Figure 8 gives $d\sigma/dp_{Tj}$ for the cuts of Eq. (1) and (3). The selective reduction of the QCD contribution due to the

more stringent E_j and $|\eta_j|$ cuts is apparent. We also see from Fig. 8(a) that without requiring a high jet energy there is no competitive cut that can be made on p_{Tj} to suppress the QCD background relative to the signal.

The $d\sigma/dp_{Tj}$ distribution in the $m_H = 0.6$ and 1 TeV cases falls more rapidly with increasing p_{Tj} than in the $m_H = 0.1$ TeV case. This result can be qualitatively understood as follows. In the case of a heavy Higgs boson the bulk of the cross section is due to $W_L W_L \rightarrow Z_L Z_L$ fusion whereas in the light Higgs case the transverse polarizations are dominant. A quark radiating a longitudinal W will exhibit a transverse momentum distribution following a dp_{Tj}^2/p_{Tj}^4 dependence, while a dp_{Tj}^2/p_{Tj}^2 dependence results from W_T radiation.¹⁸ Therefore the average p_{Tj} for W_L radiation is smaller than that for W_T radiation.

IV. COMPARISON OF JET-TAGGING AND JET-INCLUSIVE RESULTS

At this point we turn to a comparison of the single jet tagging and jet inclusive methods of detecting a heavy Higgs boson. Figure 9 shows the M_{ZZ} distributions of the signal and the QCD backgrounds for each method. With jet tagging, the signal arising from a Higgs boson of mass $m_H = 0.6$ to 1 TeV exceeds the QCD background by almost an order of magnitude. Moreover, the jet-tagged signal is manifest as either a sharp resonance shape (the $m_H = 0.6$ TeV case) or as a flat plateau (the $m_H = 1$ TeV case), allowing positive experimental identification. The corresponding jet-inclusive signal event rates are substantially larger but the QCD background is an appreciable fraction of the $m_H = 1$ TeV signal. Here a definitive identification of the signal excess becomes a questionable proposition.

The cross sections integrated over the range $M_{ZZ} > 0.5$ TeV are given in Table I. The numbers were obtained by using electroweak input parameters which are based on the measured value of the Z -mass, $M_Z = 91.17$ GeV, $\sin^2 \theta_w = 0.23$, and an effective QED coupling constant at the W scale of $\alpha(M_W) = 1/128$, which leads to a value of $M_W = 80.0$ GeV for the W boson mass. As mentioned before, the top quark mass was set to $m_t = 140$ GeV in the evaluation of the gluon fusion process.

The numbers in Table I include the branching fraction $B(ZZ \rightarrow 4\ell) = 4.4 \times 10^{-3}$ for $\ell = e$

or μ , and impose our standard acceptance cuts of $|y_Z| < 2.5$ and $p_{TZ} > \frac{1}{4}\sqrt{M_{ZZ}^2 - 4M_Z^2}$. Since the 4 lepton detection efficiency¹⁹ of ZZ events is expected to be above 90%, the numbers correspond to observable rates. For $m_H = 1$ TeV the jet-inclusive signal and QCD background are about the same size, whereas with a single high-energy-jet tag the QCD background is effectively eliminated. However, the event rate with the jet tag is reduced by a factor of 3 compared to the jet inclusive results, principally due to the elimination of the gluon fusion process that in our calculation is evaluated without additional parton emission; such contributions will increase our jet tagging signal event rate somewhat. The efficiency of our jet tag in retaining the $qq \rightarrow qqZZ$ signal is close to 70%, which is remarkably large!

An instructive measure of the virtues of jet tagging is provided by the significance of the rate increase due to the presence of a heavy Higgs boson. Table II gives the Higgs boson signal rates S for masses $m_H = 0.6, 0.8, \text{ and } 1.0$ TeV and the background rate B as determined from Table I. The signal rate is defined here as $S = \sigma(m_H) - \sigma(m_H = 0.1 \text{ TeV})$. The background rate includes both the QCD continuum processes and the electroweak background of essentially transversely polarized Z pairs which is defined as the SM rate for a light ($m_H = 100$ GeV) Higgs boson. Assuming no uncertainty in the determination of the background rate, $\sigma = S/\sqrt{B}$ gives a measure of the significance of the Higgs signal. The numbers for both the jet inclusive and the jet tag experiments are given in Table II.

However, the theoretical uncertainties of the background calculation cannot be ignored. Even when the full one-loop radiative corrections to these rates are known for both the signal and the background one may still expect a normalization uncertainty ϵ of $\mathcal{O}(30\%)$. Corresponding uncertainties will arise when trying to determine the background rate experimentally from the ZZ invariant mass spectrum at low values of M_{ZZ} . A more realistic error estimate must take this uncertainty in the background into account and leads to a considerably smaller significance $\sigma = S/\sqrt{B + (\epsilon B)^2}$ of the heavy Higgs boson signal. Results for a relative background normalization error of $\epsilon = 30\%$ are given in Table II.

Once these normalization uncertainties are taken into account, jet tagging yields a much

more significant heavy Higgs signal than the jet inclusive measurement because of the substantially improved signal to background ratio. Note that the background after single jet tagging is primarily due to the electroweak production of transverse Z bosons. A different method is required to distinguish these contributions from the $Z_L Z_L$ signal, *e.g.* by exploiting the $Z \rightarrow \ell\bar{\ell}$ decay distribution.

V. DISCUSSION AND SUMMARY

We have compared the detection of the $H \rightarrow ZZ \rightarrow 4$ charged lepton decay in jet-inclusive and jet-tagged events at the SSC. We advocate a jet tagging procedure which requires only a *single* very energetic jet ($E_j > 1$ TeV) in the forward region ($2 < |\eta_j| < 5$) in Z pair events identified by the leptonic decays of the two Z bosons. The jet-inclusive mode involves the Higgs signal from gluon-gluon and WW fusion subprocesses, whereas the jet-tag mode involves only the latter. For an $m_H \sim 1$ TeV Higgs boson, the event rate in the jet-inclusive case is 3 times that of the single jet-tag case. However, the QCD background is comparable to the signal in jet-inclusive events but the background is largely eliminated in a jet-tagged search. Thus jet tagging yields a way to detect a heavy Higgs boson or strong WW scattering effects that is almost free of QCD backgrounds.

The interpretation of the jet-inclusive search depends crucially on the QCD background normalization, which by now is calculated to $\mathcal{O}(\alpha^2\alpha_s)$ but has a K -factor of about 1.5 in the $M_{ZZ} > 500$ GeV region relevant to the Higgs boson search; until an $\mathcal{O}(\alpha^2\alpha_s^2)$ calculation is made, the theoretical uncertainty from higher orders on the background normalization is a concern. Even a 30% uncertainty drastically reduces the significance of the jet-inclusive heavy Higgs signal, while the effect is much less severe for the jet-tagged search, offsetting the liability of the reduced event sample for the latter.

Further confirmation of a heavy Higgs boson or strong WW scattering signal in the jet-tag approach is possible in the $d\sigma/dE_j$ distribution of $ZZ + 1$ jet events, which should fall steeply in the region $E_j \lesssim 500$ GeV due to the QCD contribution, and then flatten out if a Higgs signal is present.

Unless the separation of longitudinally and transversely polarized Z bosons is considered via the angular distribution of the Z decay leptons, the pair production of *transverse* Z 's via the electroweak $qq \rightarrow qqZZ$ and the gluon fusion process constitutes an irreducible physics background. Here again jet tagging provides an additional handle on identifying longitudinal weak boson scattering via the softer jet p_T spectrum as compared to transverse Z boson emission.

Single jet tagging provides an efficient method for isolating electroweak boson scattering from other sources of Z boson pairs. Thus, if a heavy Higgs boson exists, the combination of jet-tagging and jet-inclusive measurements allows the separate determination of $qq \rightarrow qqZZ$ and $gg \rightarrow ZZ$ contributions. (Note that extra parton emission in the $gg \rightarrow ZZ$ process will likely resemble the QCD background and thus be suppressed by our jet-tagging cuts). The $Ht\bar{t}$ Yukawa coupling and the HWW couplings can thereby be experimentally determined, provided that there are no other new physics contributions.

The search for a heavy Higgs boson in the $H \rightarrow ZZ \rightarrow 4$ charged lepton channel appears to be essentially rate limited when jet tagging is used (of order 10 events for 1 year running at the standard SSC luminosity of $\mathcal{L} = 10^{33}\text{cm}^{-2}\text{sec}^{-1}$). The full benefit of substantially reducing the QCD background could be realized in future runs at a higher luminosity, *e.g.* $\mathcal{L} = 10^{34}\text{cm}^{-2}\text{sec}^{-1}$. Our techniques should also be useful for isolating the Higgs signal at the LHC.²⁰

It should be emphasized that the single jet tagging method discussed here for the $ZZ \rightarrow 4$ charged lepton mode can be used in searching for other weak boson scattering processes as well. The decay mode $H \rightarrow ZZ \rightarrow \ell^+\ell^-\nu\bar{\nu}$ is one example. Since we have considered Z pair production at very high p_{TZ} , our results for the four charged lepton mode can essentially be taken over for the $\ell^+\ell^-\nu\bar{\nu}$ decay mode which has a six times larger branching fraction. Other applications of great interest include the search for strong scattering of weak bosons in the $WZ \rightarrow WZ$ or in the $WW \rightarrow WW$ channels.

Single jet tagging appears to be a powerful tool in searching for a heavy Higgs boson

or strong weak boson scattering even in the ‘gold-plated’ Higgs boson decay mode to four charged leptons. Once the Higgs boson is discovered, we expect single jet tagging to be essential to the study of the couplings of the Higgs boson and the properties of the complete longitudinal weak boson sector.

ACKNOWLEDGEMENTS

We thank U. Baur and N. Glover for making available the computer code for the $gg \rightarrow ZZ$ calculation. This research was supported in part by the University of Wisconsin Research Committee with funds granted by the Wisconsin Alumni Research Foundation, and in part by the U. S. Department of Energy under contracts No. DE-AC02-76ER00881 and No. DE-FG05-87ER40319.

APPENDIX A: AMPLITUDES FOR THE ELECTROWEAK PROCESS $qq \rightarrow qqZZ$

This appendix outlines the calculation of the cross sections for the SM electroweak processes $qq \rightarrow qqZZ$. The Feynman graphs corresponding to the two distinct processes (charged current exchange and neutral current exchange between the quark lines) are given in Figs. 10 and 11. Here we give analytic expressions for the scattering amplitudes using the methods, notation, and conventions of Refs. 9 and 14. The masses of all fermions are set to be zero.

All amplitudes are written in a way that allows one to easily deduce crossing relations. The physical momenta \bar{p}_i of the fermions are given by $p_i = s_i \bar{p}_i$ with $s_i = +1$ for quarks and $s_i = -1$ for antiquarks. Similarly the chirality indices σ_i and the physical helicities $\bar{\sigma}_i/2$ are related by $\sigma_i = s_i \bar{\sigma}_i$. We express the Feynman amplitudes in terms of (p_i, k_i, σ_i) with phase space and wave functions given in terms of the physical quantities $(\bar{p}_i, \bar{k}_i, \bar{\sigma}_i/2)$. The quark flavors are labeled by f_i and specified where necessary.

The scattering amplitudes are given in the two-component Weyl basis for spinors. A bracket notation for the spinors representing external (anti-) fermions is used. In terms of the normalized helicity eigenspinor $\chi_{\sigma_i}(\bar{p}_i)$ we define

$$\langle p_i | = \chi_{\sigma_i}^\dagger(\bar{p}_i), \quad |p_i\rangle = \chi_{\sigma_i}(\bar{p}_i). \quad (\text{A1})$$

The emission of a vector boson with momentum k_1 and polarization vector e_1^μ , from the external fermion i , is described by a unique complex two-vector which we denote by

$$\begin{aligned} \langle p_i k_1 | &= \chi_{\sigma_i}^\dagger(\bar{p}_i) (\not{e}_1)_{\sigma_i} \frac{(\not{p}_i + \not{k}_1)_{-\sigma_i}}{(p_i + k_1)^2}, \\ |k_1 p_i\rangle &= \frac{(\not{p}_i - \not{k}_1)_{-\sigma_i}}{(p_i - k_1)^2} (\not{e}_1)_{\sigma_i} \chi_{\sigma_i}(\bar{p}_i). \end{aligned} \quad (\text{A2})$$

The emission of two vector bosons with momenta k_1, k_2 and polarization vectors e_1^μ, e_2^μ from external fermion i is also described by a unique complex two-vector which we denote by

$$\begin{aligned}
\langle p_i k_1 k_2 | &= \chi_{\sigma_i}^\dagger(\bar{p}_i) (\phi_1)_{\sigma_i} \frac{(\not{p}_i + \not{k}_1)_{-\sigma_i}}{(p_2 + k_1)^2} (\phi_2)_{\sigma_i} \frac{(\not{p}_i + \not{k}_1 + \not{k}_2)_{-\sigma_i}}{(p_i + k_1 + k_2)^2}, \\
|k_2 k_1 p_i \rangle &= \frac{(\not{p}_i - \not{k}_1 - \not{k}_2)_{-\sigma_i}}{(p_i - k_1 - k_2)^2} (\phi_2)_{\sigma_i} \frac{(\not{p}_i - \not{k}_1)_{-\sigma_i}}{(p_i - k_1)^2} (\phi_1)_{\sigma_i} \chi_{\sigma_i}(\bar{p}_i).
\end{aligned} \tag{A3}$$

The triple gauge boson coupling is written in terms of the tensor

$$T^{\mu\nu\lambda}(k_1, k_2) = (k_1 - k_2)^\mu g^{\nu\lambda} + (2k_2 + k_1)^\nu g^{\mu\lambda} - (2k_1 + k_2)^\lambda g^{\mu\nu}, \tag{A4}$$

where k_1 and k_2 are four-momenta of bosons leaving the triple vertex with polarization vectors $\epsilon_{1\mu}(k_1)$ and $\epsilon_{2\nu}(k_2)$. The contraction of $T^{\mu\nu\lambda}$ with four-vectors X_μ and Y_λ will be denoted by

$$\Gamma^\mu(k_1, k_2; X, Y) \equiv T^{\mu\nu\lambda} X_\nu Y_\lambda. \tag{A5}$$

The Z coupling strength is

$$g_{\sigma_i}^Z(f) = \begin{cases} g_Z (T_{3f} - Q_f x_w) & \text{for } \sigma_i = -1, \\ g_Z (-Q_f x_w) & \text{for } \sigma_i = +1, \end{cases} \tag{A6}$$

where $g_Z = g/\cos\theta_w$, $x_w = \sin^2\theta_w$, and the γ coupling is $g_\pm^\gamma(f) = e Q_f = g \sin\theta_w Q_f$. The W -fermion coupling strength is nonzero only for chirality $\sigma_i = -1$ of the fermions,

$$g_-^W = \frac{g}{\sqrt{2}}. \tag{A7}$$

For convenience we introduce an overall factor

$$F_0 = i s_1 s_2 s_3 s_4 \delta_{\sigma_1 \sigma_2} \delta_{\sigma_3 \sigma_4} \sqrt{16 \bar{p}_1^0 \bar{p}_2^0 \bar{p}_3^0 \bar{p}_4^0}, \tag{A8}$$

and define propagator factors by

$$\begin{aligned}
D_V(q) &= \frac{1}{q^2 - M_V^2 + i M_V \Gamma_V(q)}, \\
\Gamma_V(q) &= \Gamma_V \theta(q^2), \\
P_V^{\mu\nu}(k) &= g^{\mu\nu} + \frac{(1 - \xi) k^\mu k^\nu}{\xi k^2 - M_V^2},
\end{aligned} \tag{A9}$$

where $V = W, Z$ or H , and ξ is the gauge parameter. For diagrams of Fig. 10, which involve charged current exchange the flavors of the external quarks are fixed to $q = u, c$ and $q' = s, d$.

The amplitudes are given by

$$\begin{aligned}
i\mathcal{M}^{(a)} &= -\frac{g^2}{1-x_w} M_W^2 g_{\sigma_1}^W g_{\sigma_3}^W F_0 D_W(p_1-p_2) D_W(p_3-p_4) D_H(k_1+k_2) \\
&\quad \times \epsilon(k_1) \cdot \epsilon(k_2) \langle p_2 | (\sigma^\mu)_{\sigma_1} | p_1 \rangle \langle p_4 | (\sigma_\mu)_{\sigma_3} | p_3 \rangle ,
\end{aligned} \tag{A10}$$

$$\begin{aligned}
i\mathcal{M}^{(b)} &= -g^2(1-x_w) g_{\sigma_1}^W g_{\sigma_3}^W F_0 D_W(p_1-p_2) D_W(p_3-p_4) \\
&\quad \times \left[2\epsilon(k_1) \cdot \epsilon(k_2) \langle p_2 | (\sigma^\mu)_{\sigma_1} | p_1 \rangle \langle p_4 | (\sigma_\mu)_{\sigma_3} | p_3 \rangle \right. \\
&\quad \left. - \langle p_2 | (\not{k}(k_1))_{\sigma_1} | p_1 \rangle \langle p_4 | (\not{k}(k_2))_{\sigma_3} | p_3 \rangle - \langle p_2 | (\not{k}(k_2))_{\sigma_1} | p_1 \rangle \langle p_4 | (\not{k}(k_1))_{\sigma_3} | p_3 \rangle \right] ,
\end{aligned} \tag{A11}$$

$$\begin{aligned}
i\mathcal{M}^{(c)} &= g^2(1-x_w) g_{\sigma_1}^W g_{\sigma_3}^W F_0 D_W(p_1-p_2) D_W(p_3-p_4) D_W(p_1-p_2-k_1) P_W^{\mu\nu}(p_1-p_2-k_1) \\
&\quad \times \Gamma_\mu(-k_1, p_1-p_2; \epsilon(k_1), \langle p_2 | (\sigma)_{\sigma_1} | p_1 \rangle) \Gamma_\nu(p_3-p_4, -k_2; \langle p_4 | (\sigma)_{\sigma_3} | p_3 \rangle, \epsilon(k_2)) ,
\end{aligned} \tag{A12}$$

$$\begin{aligned}
i\mathcal{M}^{(d)} &= -\frac{g^2}{1-x_w} x_w^2 M_W^2 g_{\sigma_1}^W g_{\sigma_3}^W F_0 D_W(p_1-p_2) D_W(p_3-p_4) \\
&\quad \times \frac{\xi}{\xi(p_1-p_2-k_1)^2 - M_W^2} \langle p_2 | (\not{k}(k_1))_{\sigma_1} | p_1 \rangle \langle p_4 | (\not{k}(k_2))_{\sigma_3} | p_3 \rangle ,
\end{aligned} \tag{A13}$$

$$\begin{aligned}
i\mathcal{M}^{(e)} &= g_{\sigma_1}^W g_{\sigma_3}^W F_0 D_W(p_1-p_2-k_1) P_W^{\mu\nu}(p_1-p_2-k_1) \\
&\quad \times \left[\langle p_2 | (\sigma_\mu)_{\sigma_1} | k_1 p_1 \rangle g_{\sigma_1}^Z(q'_1) + \langle p_2 k_1 | (\sigma_\mu)_{\sigma_1} | p_1 \rangle g_{\sigma_1}^Z(q_1) \right] \\
&\quad \times \left[\langle p_4 | (\sigma_\nu)_{\sigma_3} | k_2 p_3 \rangle g_{\sigma_3}^Z(q_2) + \langle p_4 k_2 | (\sigma_\nu)_{\sigma_3} | p_3 \rangle g_{\sigma_3}^Z(q'_2) \right] ,
\end{aligned} \tag{A14}$$

$$\begin{aligned}
i\mathcal{M}^{(f)} &= -g\sqrt{1-x_w} g_{\sigma_1}^W g_{\sigma_3}^W F_0 D_W(p_1-p_2-k_1) P_W^{\mu\nu}(p_1-p_2-k_1) \\
&\quad \times \left\{ D_W(p_1-p_2) \Gamma_\mu(-k_1, p_1-p_2; \epsilon(k_1), \langle p_2 | (\sigma)_{\sigma_1} | p_1 \rangle) \right. \\
&\quad \times \left[\langle p_4 | (\sigma_\nu)_{\sigma_3} | k_2 p_3 \rangle g_{\sigma_3}^Z(q_2) + \langle p_4 k_2 | (\sigma_\nu)_{\sigma_3} | p_3 \rangle g_{\sigma_3}^Z(q'_2) \right] \\
&\quad + D_W(p_3-p_4) \Gamma_\mu(p_3-p_4, -k_2; \langle p_4 | (\sigma)_{\sigma_3} | p_3 \rangle, \epsilon(k_2)) \\
&\quad \left. \times \left[\langle p_2 | (\sigma_\nu)_{\sigma_1} | k_1 p_1 \rangle g_{\sigma_1}^Z(q'_1) + \langle p_2 k_1 | (\sigma_\nu)_{\sigma_1} | p_1 \rangle g_{\sigma_1}^Z(q_1) \right] \right\} ,
\end{aligned} \tag{A15}$$

$$\begin{aligned}
i\mathcal{M}^{(g)} = & g_{\sigma_1}^W g_{\sigma_3}^W F_0 \left\{ D_W(p_1 - p_2) \langle p_2 | (\sigma^\mu)_{\sigma_1} | p_1 \rangle \left[\langle p_4 | (\sigma_\mu)_{\sigma_3} | k_1 k_2 p_3 \rangle (g_{\sigma_3}^Z(q_2))^2 \right. \right. \\
& + \left. \langle p_4 k_1 | (\sigma_\mu)_{\sigma_3} | k_2 p_3 \rangle g_{\sigma_3}^Z(q_2) g_{\sigma_3}(q'_2) + \langle p_4 k_1 k_2 | (\sigma_\mu)_{\sigma_3} | p_3 \rangle (g_{\sigma_3}^Z(q'_2))^2 \right] \\
& + D_W(p_3 - p_4) \langle p_4 | (\sigma^\mu)_{\sigma_3} | p_3 \rangle \left[\langle p_2 | (\sigma_\mu)_{\sigma_1} | k_1 k_2 p_3 \rangle (g_{\sigma_1}^Z(q'_1))^2 \right. \\
& \left. \left. + \langle p_2 k_1 | (\sigma_\mu)_{\sigma_1} | k_2 p_3 \rangle g_{\sigma_1}^Z(q'_1) g_{\sigma_1}^Z(q_1) + \langle p_2 k_1 k_2 | (\sigma_\mu)_{\sigma_1} | p_3 \rangle (g_{\sigma_1}^Z(q_1))^2 \right] \right\}. \quad (\text{A16})
\end{aligned}$$

For all diagrams except 10(a) and 10(b) the interchange of the two final state Z bosons leads to distinct new contributions, *i.e.* we have to add the matrix elements $\mathcal{M}^{(c)}$ to $\mathcal{M}^{(g)}$ with $(k_1 \leftrightarrow k_2)$ interchanged.

The second subprocess, which also contributes to ZZ production, is the neutral current exchange, given in Fig. 11. The individual Feynman diagrams contribute as follows (q_1 and q_2 can now be any flavors) :

$$\begin{aligned}
i\mathcal{M}^{(a)} = & -\frac{g^2}{(1-x_w)^2} M_W^2 g_{\sigma_1}^Z(q_1) g_{\sigma_3}^Z(q_2) F_0 D_Z(p_1 - p_2) D_Z(p_3 - p_4) D_H(k_1 + k_2) \\
& \times \epsilon(k_1) \cdot \epsilon(k_2) \langle p_2 | (\sigma^\mu)_{\sigma_1} | p_1 \rangle \langle p_4 | (\sigma_\mu)_{\sigma_3} | p_3 \rangle, \quad (\text{A17})
\end{aligned}$$

$$\begin{aligned}
i\mathcal{M}^{(b)} = & -\frac{g^2}{(1-x_w)^2} M_W^2 g_{\sigma_1}^Z(q_1) g_{\sigma_3}^Z(q_2) F_0 D_Z(p_1 - p_2) D_Z(p_3 - p_4) D_H(p_1 - p_2 - k_1) \\
& \times \langle p_2 | (\not{\epsilon}(k_1))_{\sigma_1} | p_1 \rangle \langle p_4 | (\not{\epsilon}(k_2))_{\sigma_3} | p_3 \rangle, \quad (\text{A18})
\end{aligned}$$

$$\begin{aligned}
i\mathcal{M}^{(c)} = & \sum_{V=\gamma, Z} g_{\sigma_1}^V(q_1) g_{\sigma_3}^V(q_2) (g_{\sigma_3}^Z(q_2))^2 F_0 D_V(p_1 - p_2) \langle p_2 | (\sigma^\mu)_{\sigma_1} | p_1 \rangle \\
& \times \left[\langle p_4 k_1 | (\sigma_\mu)_{\sigma_3} | k_2 p_3 \rangle + \langle p_4 | (\sigma_\mu)_{\sigma_3} | k_1 k_2 p_3 \rangle + \langle p_4 k_1 k_2 | (\sigma_\mu)_{\sigma_3} | p_3 \rangle \right] \\
& + \sum_{V=\gamma, Z} g_{\sigma_1}^V(q_1) g_{\sigma_3}^V(q_2) (g_{\sigma_1}^Z(q_1))^2 F_0 D_V(p_3 - p_4) \langle p_4 | (\sigma^\mu)_{\sigma_3} | p_3 \rangle \\
& \times \left[\langle p_2 k_1 | (\sigma_\mu)_{\sigma_1} | k_2 p_1 \rangle + \langle p_2 | (\sigma_\mu)_{\sigma_1} | k_1 k_2 p_1 \rangle + \langle p_2 k_1 k_2 | (\sigma_\mu)_{\sigma_1} | p_1 \rangle \right], \quad (\text{A19})
\end{aligned}$$

$$\begin{aligned}
i\mathcal{M}^{(d)} = & \sum_{V=\gamma, Z} g_{\sigma_1}^V(q_1) g_{\sigma_3}^V(q_2) g_{\sigma_1}^Z(q_1) g_{\sigma_3}^Z(q_2) F_0 D_V(p_1 - p_2 - k_1) P_V^{\mu\nu}(p_1 - p_2 - k_1) \quad (\text{A20}) \\
& \times \left[\langle p_2 | (\sigma_\mu)_{\sigma_1} | k_1 p_1 \rangle + \langle p_2 k_1 | (\sigma_\mu)_{\sigma_1} | p_1 \rangle \right] \left[\langle p_4 | (\sigma_\nu)_{\sigma_3} | k_2 p_3 \rangle + \langle p_4 k_2 | (\sigma_\nu)_{\sigma_3} | p_3 \rangle \right].
\end{aligned}$$

Except for $\mathcal{M}^{(a)}$, we have to add the matrix elements with $(k_1 \leftrightarrow k_2)$ interchanged.

In both the charged current and the neutral current exchange processes, the complete matrix element must be antisymmetrized in $(p_1, \sigma_1)(p_3, \sigma_3)$ or $(p_2, \sigma_2)(p_4, \sigma_4)$, when identical flavors occur on the two incoming or outgoing fermion lines (see Ref. 9 for details).

APPENDIX B: AMPLITUDES FOR THE PROCESS $q\gamma \rightarrow qZZ$

In this appendix we consider contributions to Z boson pair production from the subprocess

$$q(p_1)\gamma(q) \rightarrow q(p_2)Z(k_1)Z(k_2), \quad (\text{B1})$$

where the quark q has arbitrary flavor f . We consider this process in order to justify the use of a $Q^2(\gamma) > 5 \text{ GeV}^2$ cut on the virtuality of the exchanged photon in t -channel photon exchange in the calculation of the deep inelastic process $pp \rightarrow ZZjj$, neglecting any contribution from the low Q^2 region.

For $Q^2 \simeq 0$, the photon can be treated as on-shell, with the scattering of a quark and a photon giving a pair of Z bosons and a jet. In the low Q^2 region the photon structure function inside the proton is dominated by the elastic proton contribution¹⁶ and an excellent parametrization of the elastic ‘Weizsäcker-Williams’ distribution of the photon inside the proton is given by²¹

$$f_{\gamma/p}(x) = \frac{\alpha}{2\pi} x \left[c_1 y \ln \left(1 + \frac{c_2}{z} \right) - (y + c_3) \ln \left(1 - \frac{1}{z} \right) + \frac{c_4}{z-1} + \frac{c_5 y + c_6}{z} + \frac{c_7 y + c_8}{z^2} + \frac{c_9 y + c_{10}}{z^3} \right], \quad (\text{B2})$$

where

$$y = \frac{1}{2} - \frac{2}{x} + \frac{2}{x^2}, \quad (\text{B3})$$

$$z = 1 + \frac{a}{4} \frac{x^2}{1-x}, \quad a = \frac{4m_p^2}{0.71 \text{ GeV}^2} = 4.96, \quad (\text{B4})$$

$$\begin{aligned}
c_1 &= -2.76 \times 10^{-2}, & c_2 &= 3.96, \\
c_3 &= 13.8, & c_4 &= -2.48, \\
c_5 &= -0.891, & c_6 &= -11.3, \\
c_7 &= -0.716, & c_8 &= -4.43, \\
c_9 &= 0.238, & c_{10} &= -2.12.
\end{aligned} \tag{B5}$$

The Feynman diagrams for the process are given in Fig. 12. The scattering amplitude derived from these Feynman diagrams is

$$\begin{aligned}
i\mathcal{M} &= -is_1s_2\delta_{\sigma_1\sigma_2}\sqrt{4\bar{p}_1^0\bar{p}_2^0}g_{\sigma_1}^\gamma(f)\left(g_{\sigma_1}^Z(f)\right)^2 \\
&\times \left[\langle p_2k_1 | (\not{\epsilon}(q))_{\sigma_1} | k_2p_1 \rangle + \langle p_2 | (\not{\epsilon}(q))_{\sigma_1} | k_1k_2p_2 \rangle + \langle p_2k_1k_2 | (\not{\epsilon}(q))_{\sigma_1} | p_1 \rangle \right] + (k_1 \leftrightarrow k_2),
\end{aligned} \tag{B6}$$

where the same notation as in appendix A has been used.

At the SSC the cross-section for this process under similar cuts as the signal ($M_{ZZ} > 500$ GeV, $|y_Z| < 2.5$, $p_{TZ} > \frac{1}{4}\sqrt{M_{ZZ}^2 - 4M_Z^2}$, $E_j > 100$ GeV, $|\eta_j| < 5$) is 0.12 fb, whereas the signal ($m_H = 1$ TeV) is 390 fb. Therefore, we conclude that considering only the phase space region with $Q^2 > 5$ GeV² for t -channel photon exchange is perfectly justified.

-
- ¹R. N. Cahn *et al.*, Phys. Rev. **D35**, 1626 (1987); V. Barger, T. Han, and R. J. N. Phillips, Phys. Rev. **D37** 2005 (1988); R. Kleiss and W. J. Stirling, Phys. Lett. **200B**, 193 (1988).
- ²V. Barger, T. Han, and R. J. N. Phillips, Phys. Lett. **200B**, 193 (1988); U. Baur and E. W. N. Glover, UW-Madison preprint, MAD/PH/577, (1990).
- ³M. S. Chanowitz and M. K. Gaillard, Nucl. Phys. **B261**, 375 (1985); M. S. Chanowitz, Ann. Rev. Nucl. Part. Sci. **38**, 323 (1985); M. S. Chanowitz and M. Golden, Phys. Rev. Lett. **61**, 1053 (1988); **63**, 466(E) (1989); G. Kane and C. P. Yuan, Phys. Rev. **D40**, 2231 (1989); A. Dobado and M. J. Herrero, Phys. Lett. **B228**, 195 (1989); F. Donoghue and C. Ramire, *ibid.*, **234**, 361 (1990); A. Dobado, M. J. Herrero, and T. N. Truong, *ibid.*, **235**, 129 (1990); V. Barger, Kingman Cheung, T. Han and R. J. N. Phillips, Phys. Rev. **D42**, 3052 (1990).
- ⁴R. W. Brown and K. O. Mikaelian, Phys. Rev. **D19**, 922 (1979).
- ⁵B. Mele, P. Nason, and G. Ridolfi, CERN-TH-5890-90.
- ⁶J. Ohnemus and J. F. Owens, FSU-HEP-901212 (to appear in Phys. Rev. **D**).
- ⁷P. N. Harriman, A. D. Martin, R. G. Roberts, and W. J. Stirling, Phys. Rev. **D42**, 798 (1990).
- ⁸U. Baur, E. W. N. Glover, and J. J. van der Bij, Nucl. Phys. **B318**, 106 (1989).
- ⁹V. Barger, T. Han, J. Ohnemus, and D. Zeppenfeld, Phys. Rev. **D41**, 2782 (1990).
- ¹⁰U. Baur and E. W. N. Glover, Nucl. Phys. **B347**, 12 (1990).
- ¹¹D. A. Dicus, C. Kao, and W. W. Repko, Phys. Rev. **D36**, 1570 (1987).
- ¹²E. W. N. Glover and J. J. van der Bij, Nucl. Phys. **B321**, 561 (1989).

- ¹³D. A. Dicus, S. L. Wilson, and R. Vega, Phys. Lett. **102B**, 231 (1987).
- ¹⁴K. Hagiwara and D. Zeppenfeld, Nucl. Phys. **B274**, 1 (1986); **B313**, 560 (1989).
- ¹⁵S. Willenbrock and G. Valencia, Phys. Lett. **B247**, 341 (1990).
- ¹⁶K. Hagiwara, S. Komamiya, and D. Zeppenfeld, Z. Phys. **C29**, 115 (1985); M. Drees and D. Zeppenfeld, Phys. Rev. **D39**, 2536 (1989).
- ¹⁷This negative conclusion for double jet tagging is in agreement with that of M. H. Seymour, Cavendish Report HEP 90/25 (1990).
- ¹⁸S. Dawson, Nucl. Phys. **B249**, 42 (1985); J. F. Gunion *et al.*, UCD-91-0010 (1990), to appear in Proceedings of the 1990 Snowmass Summer Study on *Research Directions for the Decade*.
- ¹⁹W. Smith, talk given at the *SSC Physics Symposium*, Madison, Wisconsin, Feb. 1991.
- ²⁰D. Froideveaux, talk given at the *SSC Physics Symposium*, Madison, Wisconsin, Feb. 1991; S. Dimopoulos *et al.*, CERN-TH-5980-91.
- ²¹B. Kniehl, Phys. Lett. **B254**, 267 (1991).

TABLE I. SSC cross sections for 4 charged lepton ($\ell = e, \mu$) production via SM $H \rightarrow ZZ$ in units of 0.1 fb. The numbers in the table also represent appropriate event rates for one SSC year at standard luminosity of 10 fb^{-1} . The acceptance cuts $M_{ZZ} > 500 \text{ GeV}$, $|y_Z| < 2.5$, and $p_{TZ} > \frac{1}{4}\sqrt{M_{ZZ}^2 - 4M_Z^2}$ are imposed.

m_H (TeV)	Jet inclusive	Single jet tag	
	gg, qq (qq only)	$E_j > 1 \text{ TeV}$	$2 < \eta_j < 5$
0.1	13 (4)	2.6	
0.6	97 (26)	16	
0.8	56 (21)	14	
1.0	39 (17)	12	
QCD	36	1.6	

TABLE II. Significance of the Higgs boson signal at the SSC. The rates correspond to the number of 4 charged lepton ($\ell = e, \mu$) events for one SSC year at standard luminosity of 10 fb^{-1} . They are given for the Higgs signal and the QCD plus electroweak background (compare Table I). The $\epsilon = 30\%$ results assume a 30% normalization uncertainty of the background calculation.

m_H (TeV)	0.6	0.8	1.0	QCD + electroweak background
jet-inclusive events	84	43	26	49
$\sigma = S/\sqrt{B}$	12.0	6.1	3.7	
$\sigma(\epsilon = 30\%)$	5.2	2.6	1.6	
single jet-tag events	13	11	9	4.2
$\sigma = S/\sqrt{B}$	6.3	5.4	4.4	
$\sigma(\epsilon = 30\%)$	5.4	4.6	3.7	

FIGURE CAPTIONS

FIG. 1. Feynman diagrams contributing to continuum ZZ production: (a) the complete lowest order contributions, (b) representative hard gluon emission and quark-gluon fusion diagrams at $\mathcal{O}(\alpha_s)$, and (c) contributions to new subprocesses appearing at $\mathcal{O}(\alpha_s^2)$. Solid lines without arrows represent either a quark or an antiquark.

FIG. 2. Feynman diagrams leading to the $gg \rightarrow ZZ$ fusion process at the 1-loop level. Diagrams involving permutations of the external vector bosons are not shown.

FIG. 3. Feynman diagrams involved in the electroweak processes $qq \rightarrow qqZZ$. Indicative diagrams are shown representing (a) vector boson fusion, (b) t -channel photon, Z , or W exchange, and (c) s -channel electroweak boson exchange.

FIG. 4. $d^2\sigma/d|\eta_j|dE_j$ distributions at the SSC for $ZZ + 1$ jet production from (a) the QCD background, (b) the $m_H = 0.6$ TeV SM signal, and c) the $m_H = 1$ TeV SM signal. For the Higgs signal the jet is the one with the largest energy in the pseudorapidity range $|\eta_j| < 5$. The Z acceptance criteria $p_{TZ} > \frac{1}{4}\sqrt{M_{ZZ}^2 - 4M_Z^2}$, $|y_Z| < 2.5$, and $M_{ZZ} > 500$ GeV are imposed.

FIG. 5. Pseudorapidity distributions for the QCD background and the SM Higgs boson signals at the SSC for $m_H = 0.1, 0.6$, and 1 TeV for $ZZ + 1$ jet production: (a) $E_j > 100$ GeV, (b) $E_j > 500$ GeV, and (c) $E_j > 1000$ GeV. The Z acceptance criteria are the same as in Fig. 4 and $|\eta_j(\text{tag})| < 5$ is required for the jets.

FIG. 6. Energy distributions of the tagged (most energetic) jet and the secondary jet for SM Higgs boson production at the SSC for (a) $m_H = 0.1$ TeV, (b) $m_H = 0.6$ TeV, and (c) $m_H = 1$ TeV. The Z acceptance criteria are as in Fig. 4 and $|\eta_j(\text{tag})| < 5$ is required for the jets.

FIG. 7. (a) Differential energy distribution of the tagged jet at the SSC and (b) the integrated cross section $\sigma(E_j(\text{tag}) > E_j(\text{cut}))$ vs. $E_j(\text{cut})$ for the tagged jet energy above a specified value $E_j(\text{cut})$. The SM Higgs signals for $m_H = 0.1, 0.6,$ and 1 TeV are shown along with the QCD background; in all cases $2 < |\eta_j(\text{tag})| < 5$ is required.

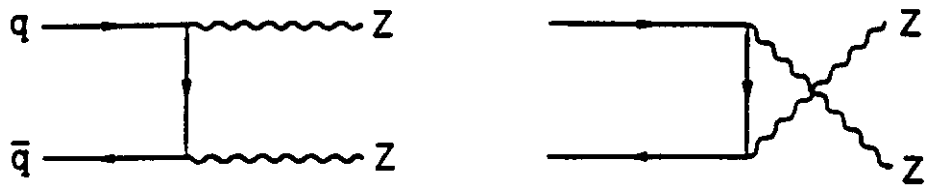
FIG. 8. Transverse momentum distribution of the tagged jet in Higgs signal and QCD background in $ZZ + 1\text{jet}$ events, with (a) $E_j(\text{tag}) > 100$ GeV and $|\eta_j(\text{tag})| < 5$, and (b) $E_j(\text{tag}) > 1000$ GeV and $2 < |\eta_j(\text{tag})| < 5$.

FIG. 9. Comparison of the M_{ZZ} invariant mass distribution for single jet tagging with $E_j > 1$ TeV, (a) and (c), and for jet-inclusive events, (b) and (d). The $m_H = 0.1$ TeV line represents the electroweak background; it has not been subtracted from any of the signal curves (solid lines). The QCD continuum background is shown separately in (a) and (b) (dashed lines) and has been added to the signal distributions in (c) and (d). In (b) the next-to-leading-order (N-L-O) calculation of the continuum QCD background from Ref. 6 is shown.

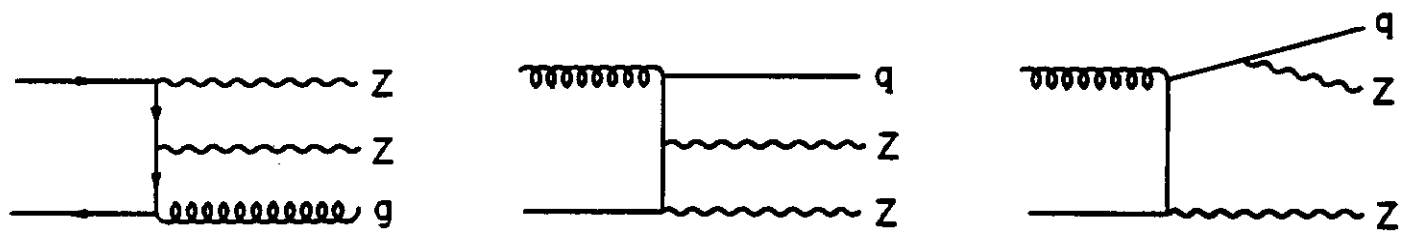
FIG. 10. Feynman graphs for the electroweak $qq \rightarrow qqZZ$ process at order α^4 involving charged current exchange only. In (c)–(g) the diagrams with the two Z -bosons interchanged are not shown.

FIG. 11. Feynman graphs for the electroweak $qq \rightarrow qqZZ$ process at order α^4 involving neutral current exchange. In (b)–(d) the diagrams with the two Z -bosons interchanged are not shown.

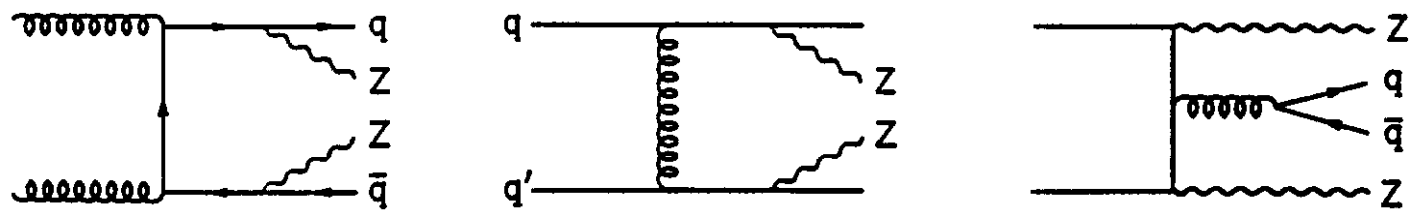
FIG. 12. Feynman graphs for the process $q\gamma \rightarrow qZZ$. Corresponding diagrams with the two Z -bosons interchanged are not shown.



(a)



(b)



(c)

Fig. 1

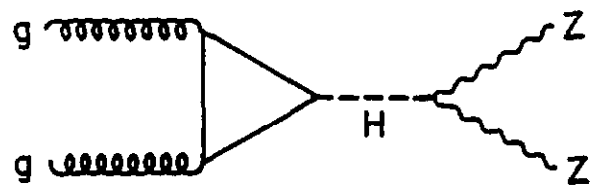
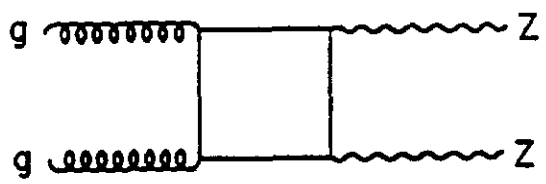
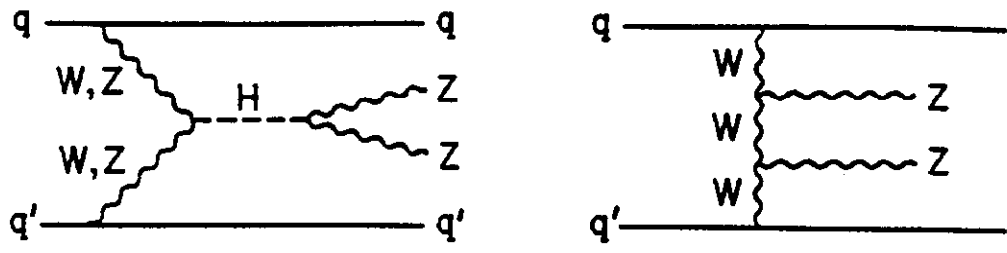
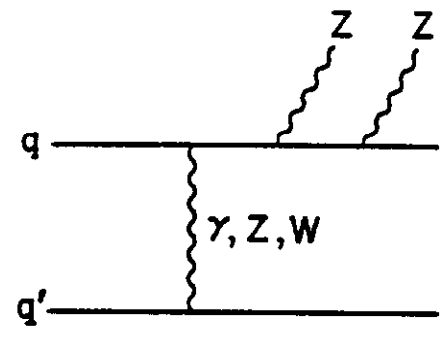


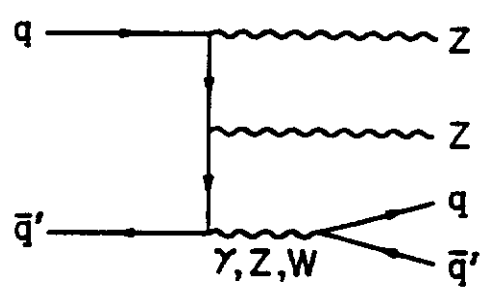
Fig. 2



(a)



(b)



(c)

Fig. 3

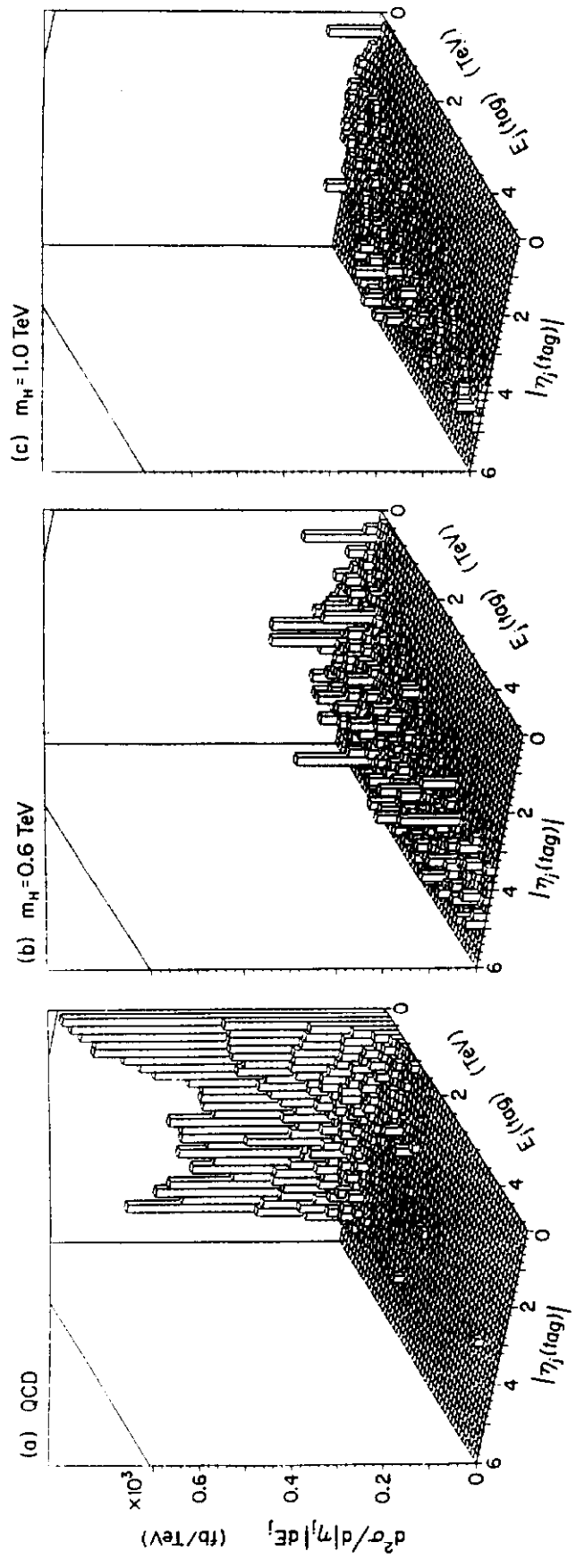


Fig. 4

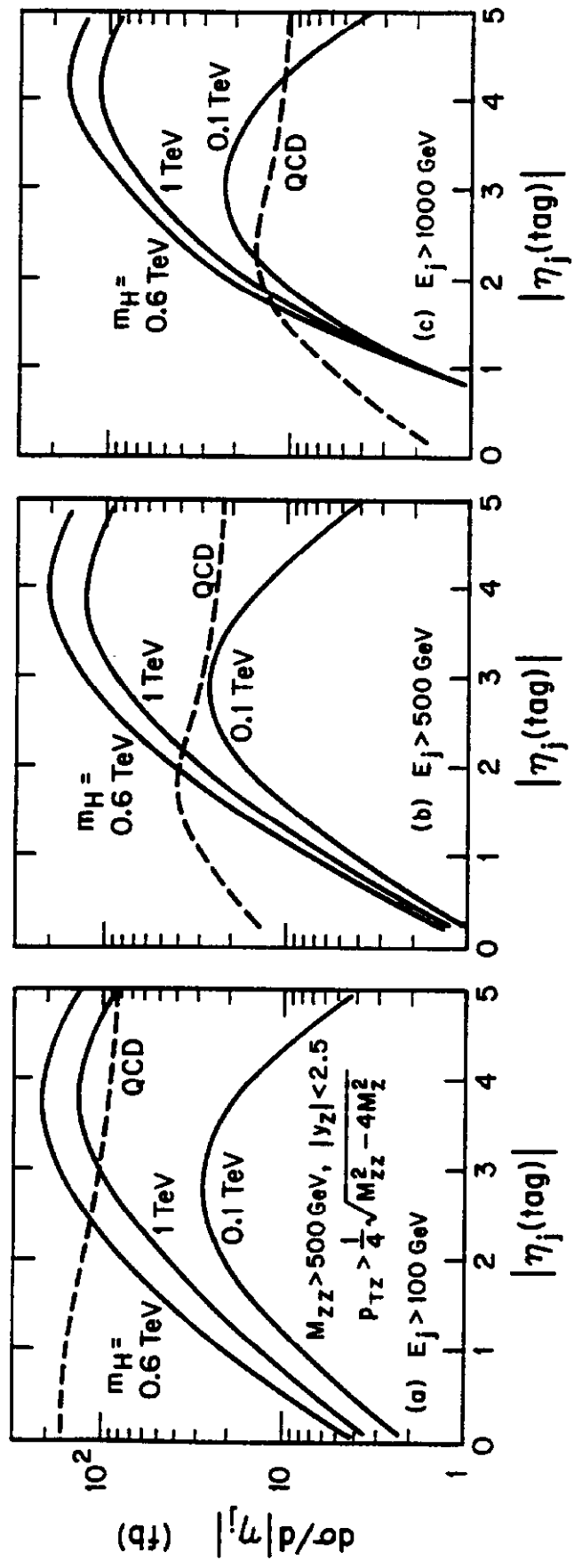


Fig. 5

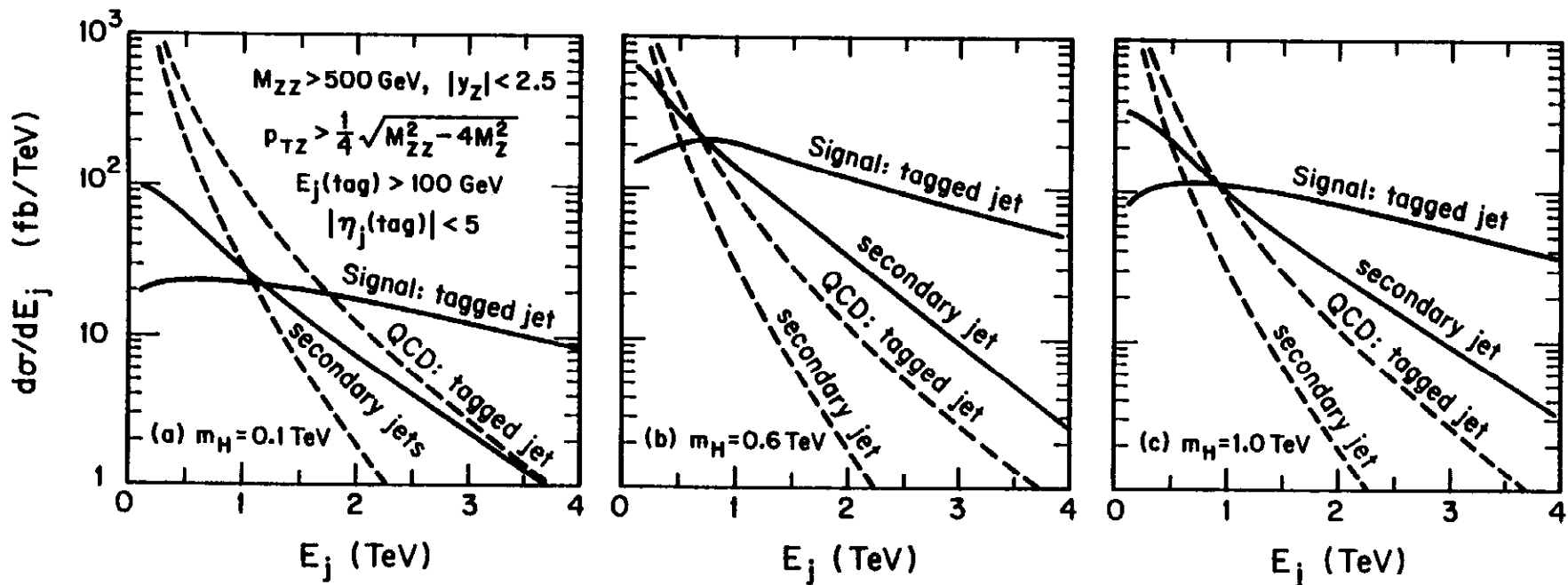


Fig. 6

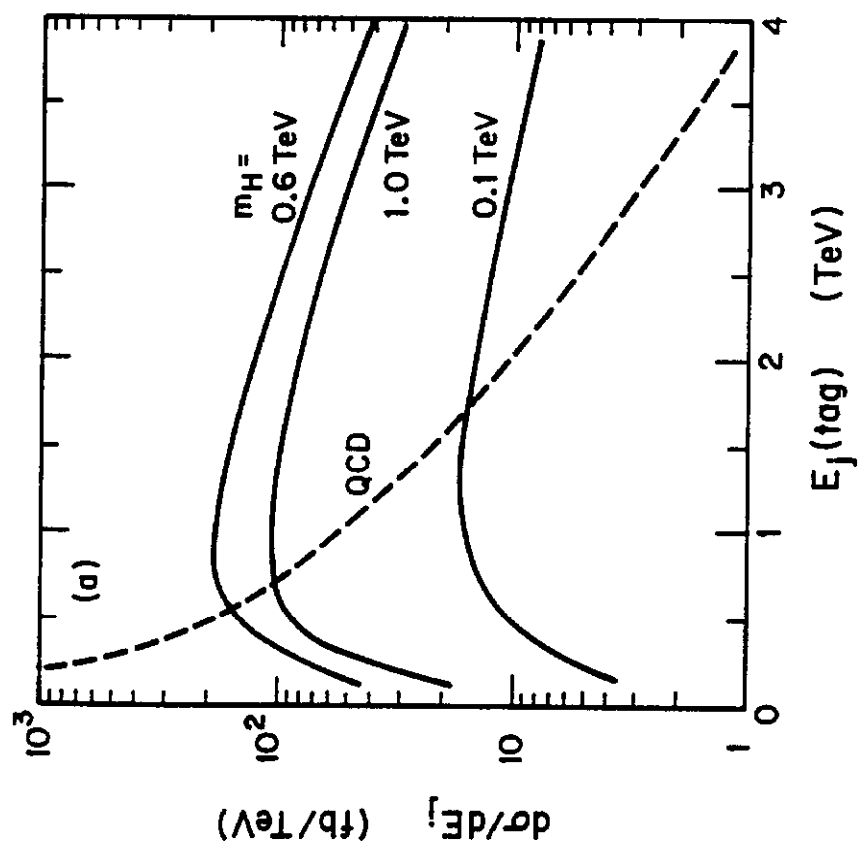
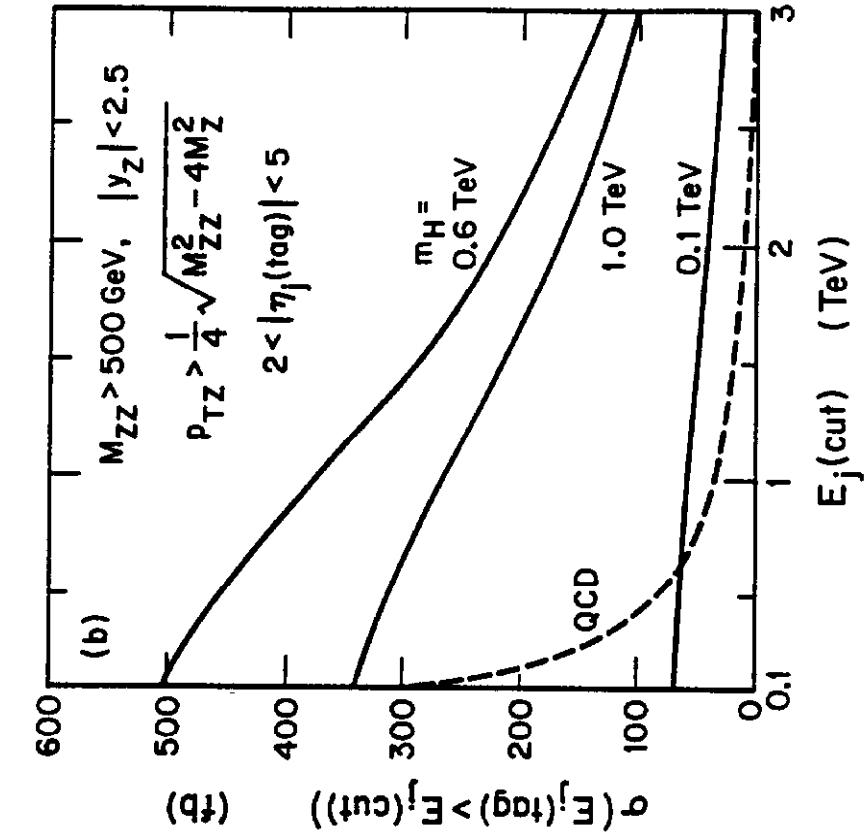


Fig. 7

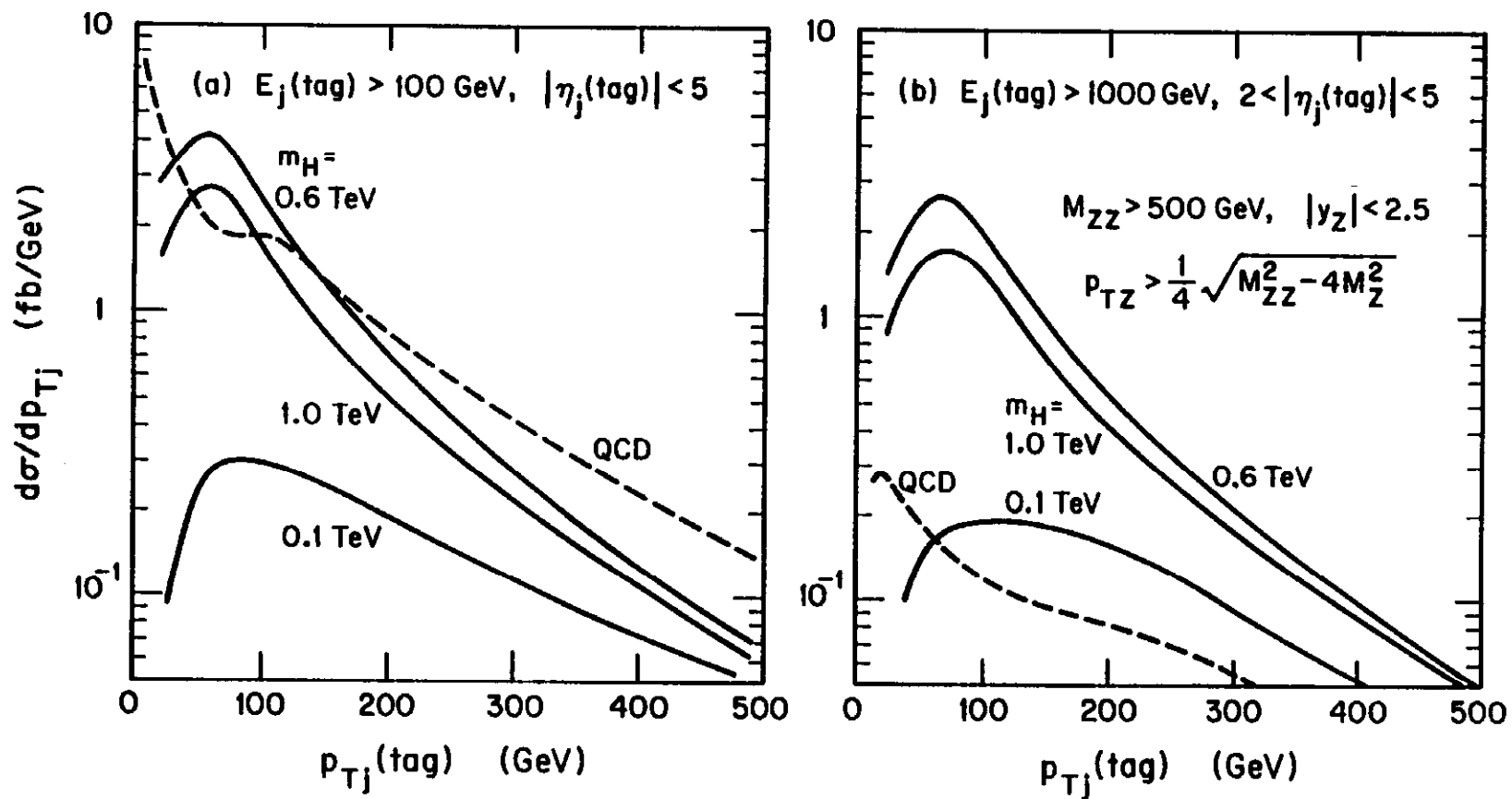


Fig. 8

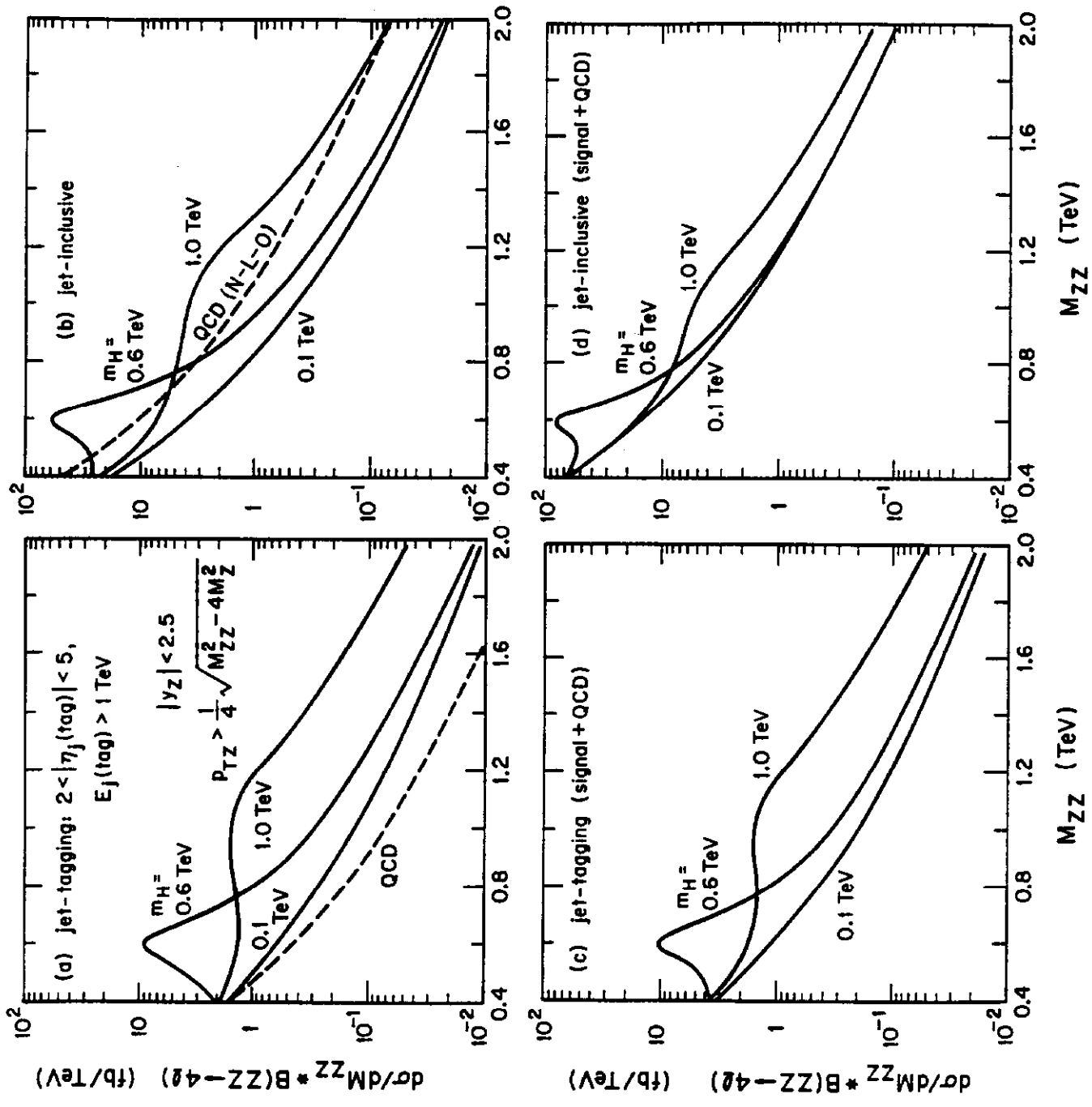


Fig. 9

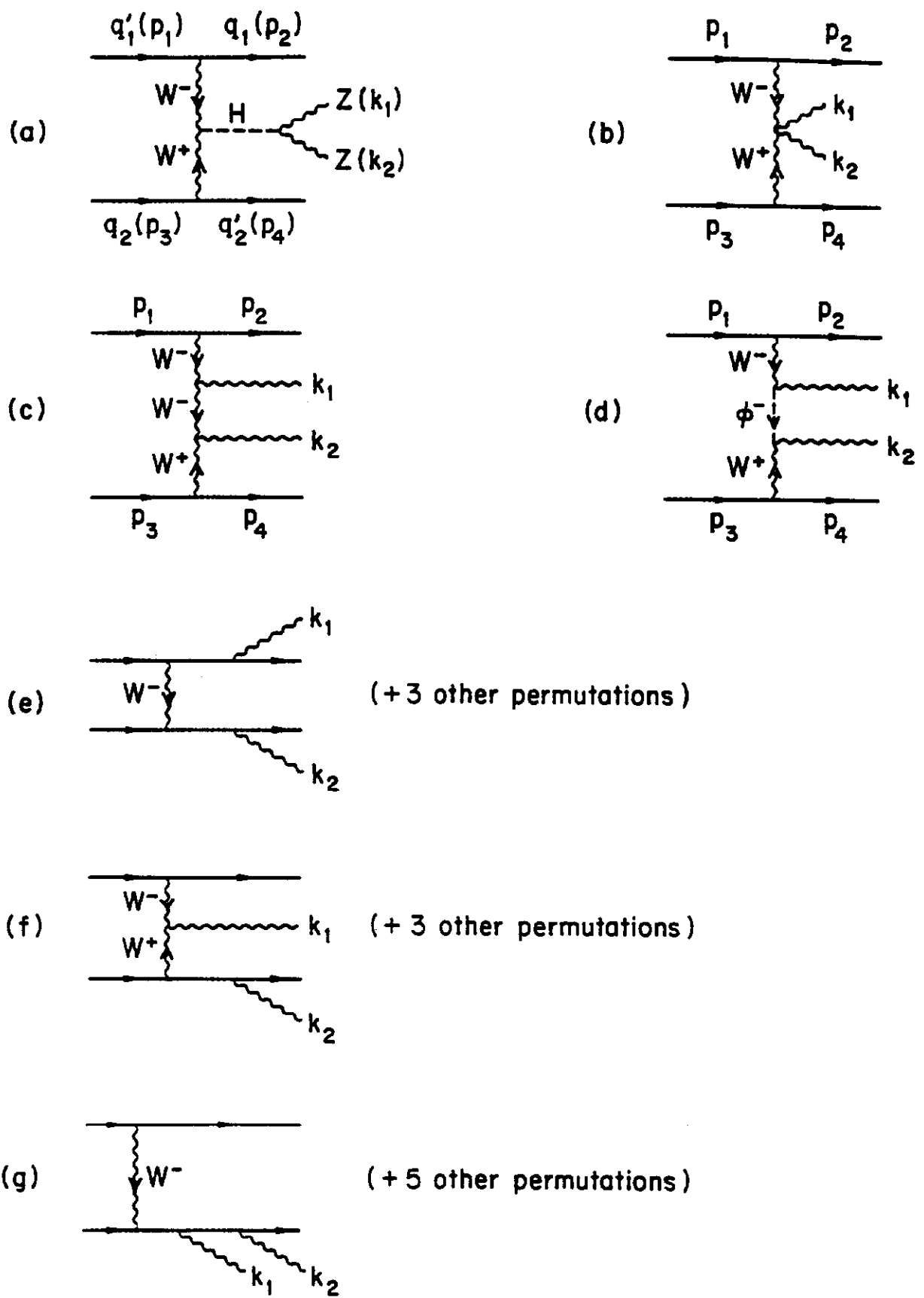


Fig. 10

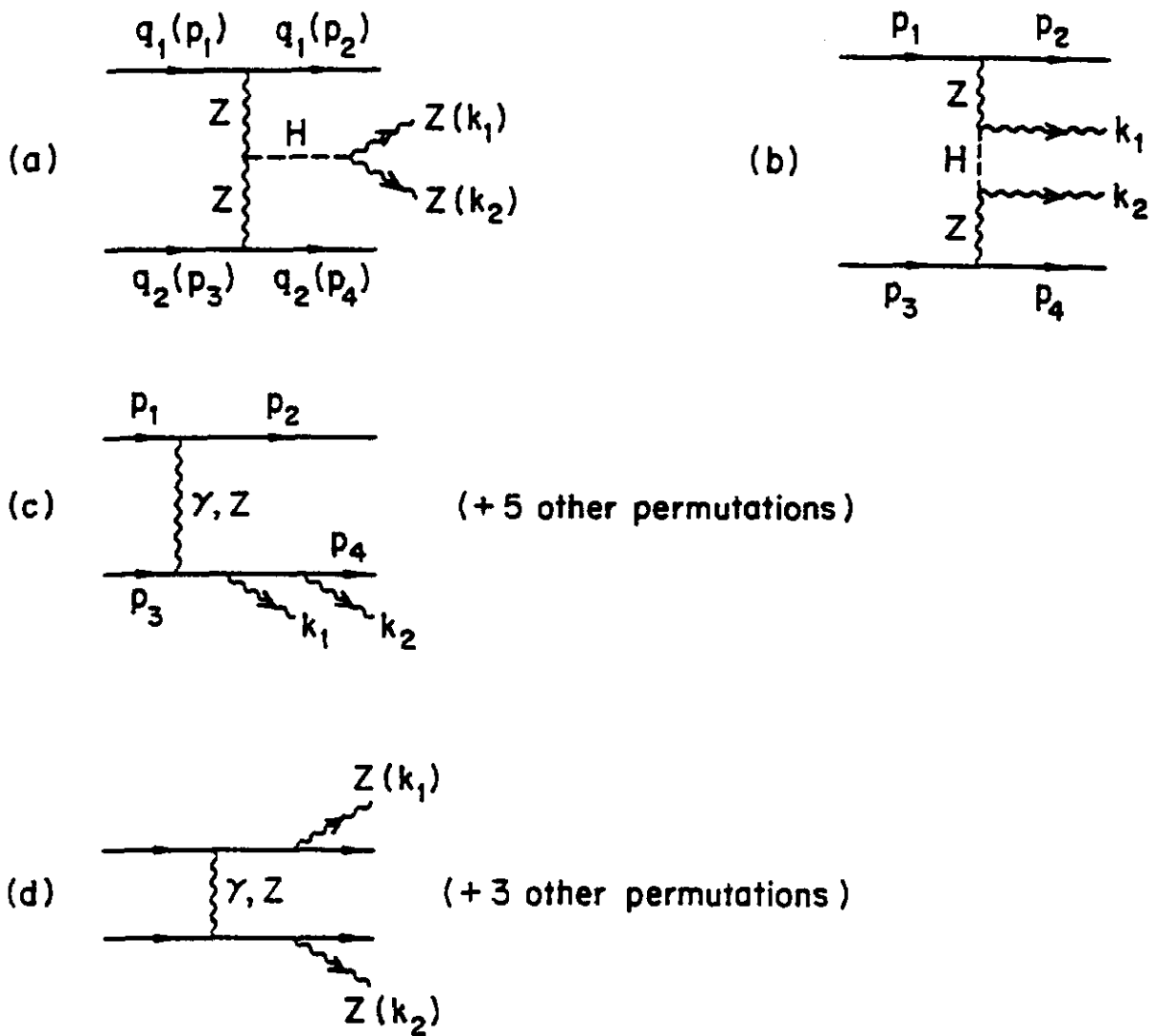


Fig. 11

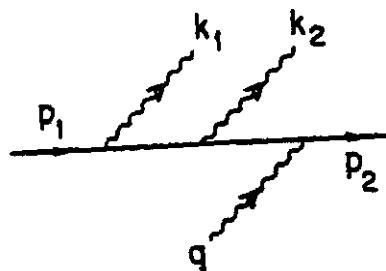
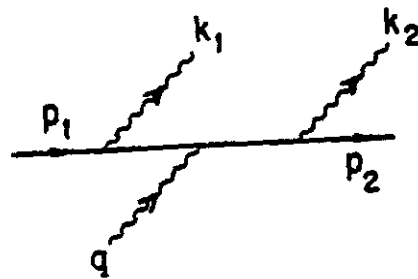
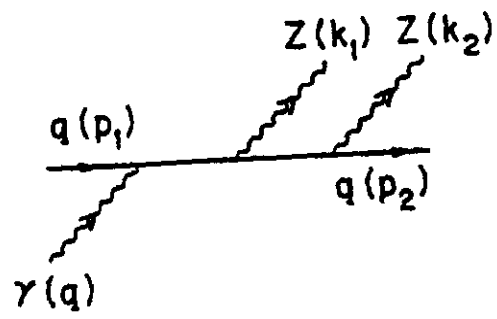


Fig. 12